Radiology

ORIGINAL RESEARCH • NEURORADIOLOGY

Detecting Large Vessel Occlusion at Multiphase CT Angiography by Using a Deep Convolutional Neural Network

Matthew T. Stib, MD • Justin Vasquez, MS • Mary P. Dong • Yun Ho Kim • Sumera S. Subzwari • Harold J. Triedman • Amy Wang • Hsin-Lei Charlene Wang, BA • Anthony D. Yao, BS • Mahesh Jayaraman, MD • Jerrold L. Boxerman, MD, PhD • Carsten Eickhoff, PhD • Ugur Cetintemel, PhD • Grayson L. Baird, PhD • Ryan A. McTaggart, MD

From the Departments of Diagnostic Imaging (M.T.S., M.J., J.L.B., G.L.B., R.A.M.), Diagnostic Imaging (A.D.Y.), and Neurosurgery (M.J., R.A.M.), Warren Alpert School of Medicine at Brown University, Rhode Island Hospital, 593 Eddy St, APC 701, Providence, RI 02903; Department of Computer Science, Brown University, Providence, RI (J.V., M.P.D., Y.H.K., S.S.S., H.J.T., A.W., H.L.C.W., C.E., U.C.); and the Norman Prince Neuroscience Institute, Rhode Island Hospital, Providence, RI (M.J., R.A.M.). Received February 12, 2020; revision requested April 6; final revision received July 30; accepted August 14. **Address correspondence to** R.A.M. (e-mail: *ryan.mctaggart@lifespan.org*).

Conflicts of interest are listed at the end of this article.

See also the editorial by Ospel and Goyal in this issue.

Radiology 2020; 00:1–10 • https://doi.org/10.1148/radiol.2020200334 • Content codes: NR IN CT

Background: Large vessel occlusion (LVO) stroke is one of the most time-sensitive diagnoses in medicine and requires emergent endovascular therapy to reduce morbidity and mortality. Leveraging recent advances in deep learning may facilitate rapid detection and reduce time to treatment.

Purpose: To develop a convolutional neural network to detect LVOs at multiphase CT angiography.

Materials and Methods: This multicenter retrospective study evaluated 540 adults with CT angiography examinations for suspected acute ischemic stroke from February 2017 to June 2018. Examinations positive for LVO (n = 270) were confirmed by catheter angiography and LVO-negative examinations (n = 270) were confirmed through review of clinical and radiology reports. Preprocessing of the CT angiography examinations included vasculature segmentation and the creation of maximum intensity projection images to emphasize the contrast agent–enhanced vasculature. Seven experiments were performed by using combinations of the three phases (arterial, phase 1; peak venous, phase 2; and late venous, phase 3) of the CT angiography. Model performance was evaluated on the held-out test set. Metrics included area under the receiver operating characteristic curve (AUC), sensitivity, and specificity.

Results: The test set included 62 patients (mean age, 69.5 years; 48% women). Single-phase CT angiography achieved an AUC of 0.74 (95% confidence interval [CI]: 0.63, 0.85) with sensitivity of 77% (24 of 31; 95% CI: 59%, 89%) and specificity of 71% (22 of 31; 95% CI: 53%, 84%). Phases 1, 2, and 3 together achieved an AUC of 0.89 (95% CI: 0.81, 0.96), sensitivity of 100% (31 of 31; 95% CI: 99%, 100%), and specificity of 77% (24 of 31; 95% CI: 59%, 89%), a statistically significant improvement relative to single-phase CT angiography (P = .01). Likewise, phases 1 and 3 and phases 2 and 3 also demonstrated improved fit relative to single phase (P = .03).

Conclusion: This deep learning model was able to detect the presence of large vessel occlusion and its diagnostic performance was enhanced by using delayed phases at multiphase CT angiography examinations.

Online supplemental material is available for this article.

Acute stroke care changed dramatically in 2015 with the publication of several randomized control trials demonstrating that endovascular therapy is more effective than alteplase alone for large vessel occlusion (LVO) stroke (1–7). Furthermore, the endovascular therapy treatment effect is profoundly time dependent, and every minute that we work faster to achieve vessel recanalization we can provide the gift of a week of disability-free life to patients (8). LVO stroke is a medical diagnosis that cannot be missed and must be made quickly.

One of the commonly used methods to confirm or exclude the presence of a LVO quickly is with CT angiography, a 3-minute examination that can easily be performed following the noncontrast head CT that is standard of care for all acute stroke imaging (9–11). Multiphase CT angiography is a protocol recently introduced for acute stroke imaging that aims to both improve LVO detection and improve patient selection for endovascular therapy (12–14).

Recent advances in deep learning, a class of machine learning, inspired new research on the uses of convolutional neural networks to perform at high levels in computer vision problems (15). These architectures hold great promise for enhancing the workflow in radiology. Specifically, in the neuroradiology domain, deep learning has been used to segment microhemorrhages at MRI with a sensitivity greater than 93% (16), to automate identification and to segment ischemic brain lesions on diffusion-weighted MRI scans (17), to detect early ischemic infarct at noncontrast CT with precision similar to diffusion-weighted MRI (18), and to detect intracranial hemorrhage at CT by reducing the time to diagnosis by 96% (19).

Abbreviations

AUC = area under the receiver operating characteristic curve, CI = confidence interval, ICA = internal carotid artery, LVO = large vessel occlusion

Summary

A deep learning model was developed to accurately detect large vessel occlusions at multiphase CT angiography imaging examinations.

Key Results

- A convolutional neural network trained to detect large vessel occlusions (LVOs) at multiphase CT angiography achieved an area under the curve of 0.89 and a sensitivity of 100% (31 of 31).
- The combinations of first and third phases, second and third phases, and all phases of the multiphase CT angiography resulted in higher detection of LVO relative to single phase.

Given the success of deep learning applications in other brain pathology, this study aimed to evaluate the feasibility of the use of convolutional neural networks to detect acute LVOs at CT angiography. It is hypothesized that a convolutional neural network can achieve a minimum area under the receiver operating characteristic curve (AUC) value of 0.70 relative to chance (0.50) by using CT angiography single-phase (arterial) imaging alone in detecting LVO. In addition, it is also hypothesized that, relative to single-phase CT angiography, the use of additional CT angiography phases (ie, venous and late venous phases) will improve diagnostic performance as defined by AUC.

Materials and Methods

Data Set Collection

Our institutional review board approved this multicenter retrospective Health Insurance Portability and Accountability Act–compliant study and waived the requirement for written informed consent.

CT angiographic images were extracted from the picture archiving and communication system at our institution from 311 unique consecutive patients with LVO from February 2017 to June 2018. Among those, 270 patients were found to contain complete multiphase CT angiography data. CT angiographic examinations were performed at three hospitals with a variety of scanners and scanning techniques. All of the patients with LVO at multiphase CT angiography were confirmed at cerebral angiography within our tertiary referral hospital's neurointerventional department. There was no exclusion of patients positive for LVO who had additional reported pathology such as stenoses of nonoccluded brain and neck vasculature.

Consecutive patients without LVO were found through a query of our institution's radiology information system specifying the CT angiography brain and neck IMG code for CT angiography ELVO (Montage; Nuance Communications, Burlington, Mass). The CT angiography emergent LVO code is reserved for patients in which a so-called code stroke was clinically initiated because of symptoms that were concerning for acute ischemic stroke. The search included the same dates (February 2017 to June 2018) as LVO-positive studies. A total of 686 unique patients negative for LVO with multiphase CT angiography were found from the same three local hospitals as the population positive for LVO. To create an equal balance of cases for model training, 270 of 686 patients were randomly selected from the cohort negative for LVO. The only exclusion criteria for patients negative for LVO other than the presence of LVO was age younger than 18 years. Otherwise, the patients negative for LVO contained a variety of non-LVO pathology such as hemodynamically and nonhemodynamically significant atherosclerotic stenoses of the cervical and intracranial vasculature and acute ischemic and hemorrhagic infarcts. Inclusion of these pathologies helped to augment the generalizability of our model. See Table 1 for demographic data.

Annotation

Patients who were positive for LVO and negative for LVO were confirmed by reviewing the radiology reports (by board-certified radiologists) and LVO-positive cases were further compared with the subsequent cerebral angiographic reports (by neurointerventional radiologists) found in the medical records available on our hospital information system (Epic, Verona, Wis).

For the purposes of this study, LVO included both anterior and posterior circulation occlusions. An anterior LVO involved the cervical internal carotid artery (ICA), intracranial ICA (from the petrous segment to the bifurcation), middle cerebral artery including the M1 and M2 portions, and tandem occlusions (ICA and middle cerebral artery). The M1–middle cerebral artery was defined as the portion of the middle cerebral artery extending from the ICA bifurcation to the bifurcation/trifurcation and the M2–middle cerebral artery was defined as branches distal to this that were oriented within the Sylvian fissure. A posterior LVO included basilar and intracranial vertebral artery occlusions.

Data Split

The total data set included 540 multiphase CT angiography examinations with an 80%/10%/10% split for training/validation/test (424, 54, and 62 examinations, respectively) (Fig 1). The patients in the test set were held out and not included in training or validation to ensure generalizability for unseen data. Each split contained a randomly selected split of LVO-positive versus LVO-negative cases. For the LVO-negative cases, we used the undersampling technique to alleviate the class imbalance problem common to real-world machine learning problems (20). LVO-positive cases were randomly balanced between right-sided occlusions versus LVOs. Because of the relatively small number of posterior circulation occlusions, they were separately and randomly split with an 80%/10%/10% (training/validation/test) distribution.

Multiphase CT Angiography

Multiphase CT angiography is a validated tool used to triage patients suspected of having acute ischemic stroke (12,13). The CT angiography examinations in our study were performed with multiple different CT scanners across three different hospitals; therefore, exact scanning parameters differed slightly across patients. Generally, a standard noncontrast CT image of the brain was first acquired, followed by the first CT angiography phase, P1, which was acquired from the aortic arch to vertex during peak arterial phase. The following two phases, P2 and

P3, were acquired from the skull base to vertex with peak venous timing (at P2) and late venous timing (at P3). Standard CT angiography protocol included a 0.625–1-mm slice thickness image acquisition reconstructed as maximum intensity projections at 24-mm slice thickness with 4 mm of spacing. We used a total of 80 mL of contrast agent (Omnipaque; Mallinckrodt, St Louis, Mo), injected at a rate of 4 mL per second.

Table 1: Demographics

Parameter	Training Cohort (n = 424)	Validation Cohort (n = 54)	Test Cohort (n = 62)
Negative for LVO	212	27	31
Mean age (y)	70.8 ± 12.9	74.4 ± 13.2	69.4 ± 14.5
Women	122 (57.5)	16 (59.3)	15 (48.4)
Positive for LVO	212	27	31
Mean age (y)	74.2 ± 14.4	77.2 ± 13.7	69.6 ± 14.0
Women	117 (55.2)	14 (51.9)	15 (48.4)
Anterior circulation	203 (95.8)	24 (88.9)	27 (87.1)
Right ICA	14 (6.9)	2 (8.3)	4 (14.8)
Right M1	49 (24.1)	7 (29.2)	7 (25.9)
Right M2	13 (6.4)	3 (12.5)	2 (7.4)
Right ICA and MCA	18 (8.9)	0	2 (7.4)
Left ICA	12 (5.9)	0	1 (3.7)
Left M1	48 (23.6)	5 (20.8)	6 (22.2)
Left M2	32 (15.8)	4 (16.7)	5 (18.5)
Left ICA and MCA	17 (8.4)	0	2 (7.4)
Posterior circulation	9 (4.2)	3 (11.1)	2 (6.5)
Basilar	5 (55.6)	1 (33.3)	2 (100)
Vertebral	4 (44.4)	2 (66.7)	0

Note.—Data in parentheses are percentages. Mean age is ± standard deviation. M1 indicates the M1 branch of the middle cerebral artery (MCA); M2 indicates the M2 branch of the MCA; left internal carotid artery (ICA) and MCA indicates tandem occlusion involving the ICA and either M1 or M2; and posterior circulation indicates the basilar or vertebral artery. LVO = large vessel occlusion.

Data Preprocessing and Vascular Segmentation

Each multiphase CT angiography examination underwent a series of preprocessing steps before it was used as input to the convolutional neural network models by using Python (version 3.6; Python Software Foundation, Wilmington, Del). Each CT angiography examination was converted from Digital Imaging and Communications in Medicine format to a NumPy array (*https://numpy.org*) and isotropic resampling was performed to standardize each voxel into a volume of 1 mm^3. Each axial CT slice was resized to 500 × 500 pixels, converted to gray scale, and normalized to values between 0 and 1.

Given the relatively small size of our data set for a deep learning application, we increased the signal-to-noise ratio by adapting a heuristic retinal vascular segmentation algorithm (21) to segment the intracranial vasculature system (ie, signal) from the underlying nonvasculature structure such as the brain parenchyma and skull (ie, noise). We did not have to significantly alter the approach adapted from retinal vessel segmentation to our data. The only major exception to the retinal vessel heuristic workflow was not requiring retinal fundus extraction by using red, blue, and green values. Otherwise, the backbone iterative process of edge detection was similar, whereby a central pixel intensity was compared with its surrounding pixel neighborhood. If the pixel intensity was greater than 50% of the surrounding pixels, then that pixel was assumed to belong to a blood vessel. Additional processing with connected components, thresholding and Sobel filtering was performed. Overall, this segmentation process took approximately 40 seconds per CT angiography scan.

We created an algorithm to select the 40 most-cranial axial images of each multiphase CT angiography examination, extending from the skull vertex through to the circle of Willis, to include all the relevant intracranial vasculature. A final preprocessing step included producing a maximal intensity projection along the axial plane of these 40 slices, resulting in a final two-dimensional maximum intensity projection image to be used in model training. This segmentation process was performed for each of the three multiphase CT angiography series, P1, P2, and P3 (Fig 2).

Model Training and Testing

After testing a variety of other models including Xception, ResNet-50, VGG16, and InceptionV3 (22–25), we adapted the DenseNet-121 (26) architecture as it produced the highest preliminary accuracies. Models were initiated with pretrained weights from ImageNet (15). All models were built by using the Keras toolkit in Python (*http://keras.io*). The learning rate was .00001 and the number of epochs until convergence was 10 with batch sizes of three. The output was a binary classifier with two output classes, LVO negative and LVO positive. All experiments were performed on a 64-bit Linux operating system (Debian 9) with 12-core central processing unit with 256-GB random-access memory, or RAM, and four graphics processing units (GTX 1080ti; Nvidia, Santa Clara, Calif; 3584 CUDA [compute unified device architecture] cores and 11 GB of GDDR5 [graphic double date rate type five synchronous dynamic random-access memory]).

A total of seven combinations of convolutional neural network model experiments were created by training on different subsets and permutations of the multiphase CT angiography data, including each phase alone (P1, P2, P3) and in various combinations (P1 and P2, P1 and P3, P2 and P3, and P1 and P2 and P3).

To help view the model's class discrimination, we used the gradient-weighted class activation mapping (Grad-CAM) approach to generate a localization map of the most important regions in an image (27). Examples of these gradient-weighted class activation mapping approaches are demonstrated in Figures 3 and 4. The source code used for modeling can be found online (*https://github.com/brown-ELVO/ELVO-dectection/commit/ae68261b92191d233a9fa9a92418aaa0cd912b74*).

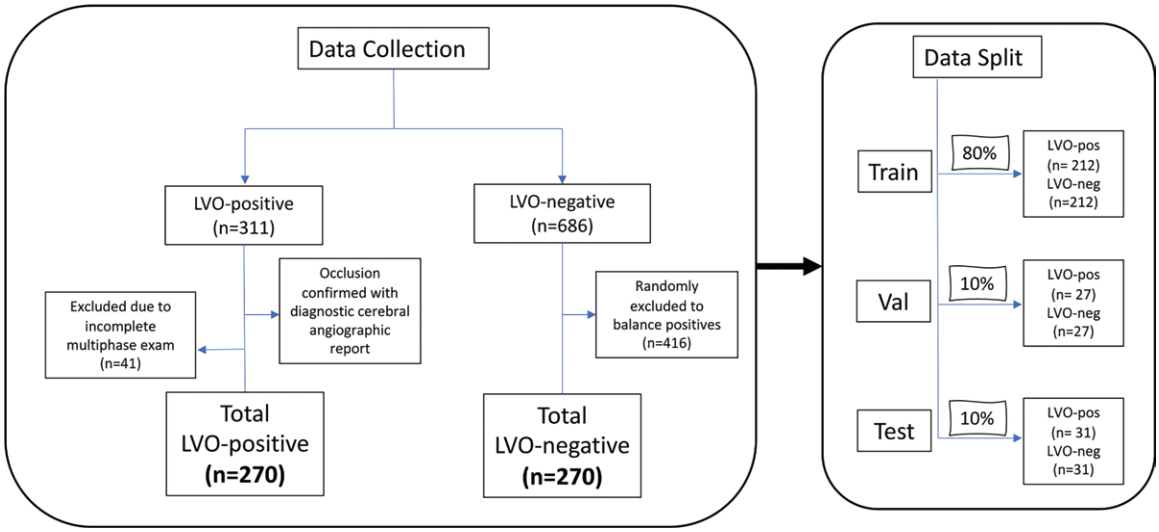

Figure 1: Flowchart demonstrates data collection and split. Consecutive multiphase CT angiography examinations in patients with and without large vessel occlusion (LVO) were collected. LVO-positive (pos) patients were excluded if there was an incomplete multiphase CT angiography study. The LVO-negative (neg) patients were balanced to the positive cases and were age and sex matched. The final data split corresponded to 80%, 10%, and 10% (training, validation [val], and test, respectively) with each split containing an equal number of patients positive and negative for LVO.

Statistical Analysis

Diagnostic performance was evaluated on the validation and test sets by using statistical software (SAS, version 9.4; SAS, Cary, NC). Sensitivity, specificity, and AUC were compared and estimated for each phase combination by using the LOGISTIC procedure. Comparisons between AUCs were assessed by using the DeLong method assuming correlation in observations. Model fit was evaluated by using the Hosmer-Lemeshow goodness-of-fit test. Youden index was used to identify the optimal cutoffs for sensitivity and specificity in the validation set. These cutoffs were then used to evaluate the test set. AUCs without cutoffs were also examined for both the validation and test sets. The test set was powered equally for sensitivity and specificity (50 and 50). Assuming a minimum AUC of 0.70 (compared with 0.50) and a type I error rate of 0.05, a test set of 31 cases and 31 control patients were required to achieve power at 80%. Power analysis was performed by using R version 3.6.1 and the pROC package version 1.15.3 (in R; *https://www.r-project.org*). The test set was completely held out and never modified. Statistical significance was set at .05 and confidence intervals (CIs) were calculated at 95%. Statistical analyses were conducted by the statistical author (G.L.B., with 8 years of experience).

Results

Detailed demographics for our training, validation, and test sets are shown in Table 1. Among the total 540 unique patients who underwent a multiphase CT angiography examination, 270 were negative for LVO (153 women and 117 men) and 270 were positive for LVO (146 women and 124 men). Average age and standard deviation for patients negative for LVO and positive for LVO were 71 years ± 15 (standard deviation) and 74 years ± 14, respectively. The held-out test set contained 29 anterior circulation occlusions (four right ICA, one left ICA, seven right M1, six left M1, two right M2, five left M2, two right tandem, two left tandem) and two posterior circulation occlusions (two basilar artery).

As indicated in Table 2 (ie, test set), all models performed above an AUC of 0.70. Phase 1 alone achieved an AUC of 0.74 (95% CI: 0.63, 0.85) with sensitivity of 24 of 31 (77%; 95% CI: 59%, 89%) and specificity of 22 of 31 (71%; 95% CI: 53%, 84%) ($P < .01$; relative to AUC of 0.5). When all phases were used (1, 2, and 3), the AUC increased to 0.89 (95% CI: 0.81, 0.96), with sensitivity of 31 of 31 (100%; 95% CI: 99%, 100%) and specificity of 24 of 31 (77%; 95% CI: 59%, 89%), a statistically significant improvement relative to single phase CT angiography ($P = .01$). When using phase 1 and 3 and 2 and 3, the AUCs achieved a value of 0.85 (95% CI: 0.77, 0.94) with sensitivity of 31 of 31 (100%) and specificity of 22 of 31 (71%; 95% CI: 53%, 84%) and with sensitivity of 26 of 31 (84%; 95% CI: 66%, 93%) and specificity of 27 of 31 (87%; 95% CI: 70%, 95%), respectively (both $P = .03$). When all other combinations of phases were used, AUC was higher than when single phase alone was used, but these differences failed to be statistically significant.

To be thorough, we also included the results from our validation set. The diagnostic performance results for the test set largely confirm the diagnostic performance of the validation set, with one exception: when phase 2 and 3 was used, the AUC achieved a value of 0.81 (95% CI: 0.71, 0.92) with sensitivity of 23 of 27 (85%; 95% CI: 66%, 94%) and specificity of 22 of 27 (81%; 95% CI: 62%, 92%); this increase failed to be statistically significant ($P = .20$).

In addition, the convolutional neural network was refined by using the validation set. Thus, the convolutional neural network's performance on the test set after being refined by using the validation set can be evaluated with the AUC as a function without optimal cutoff points; these overall AUCs without

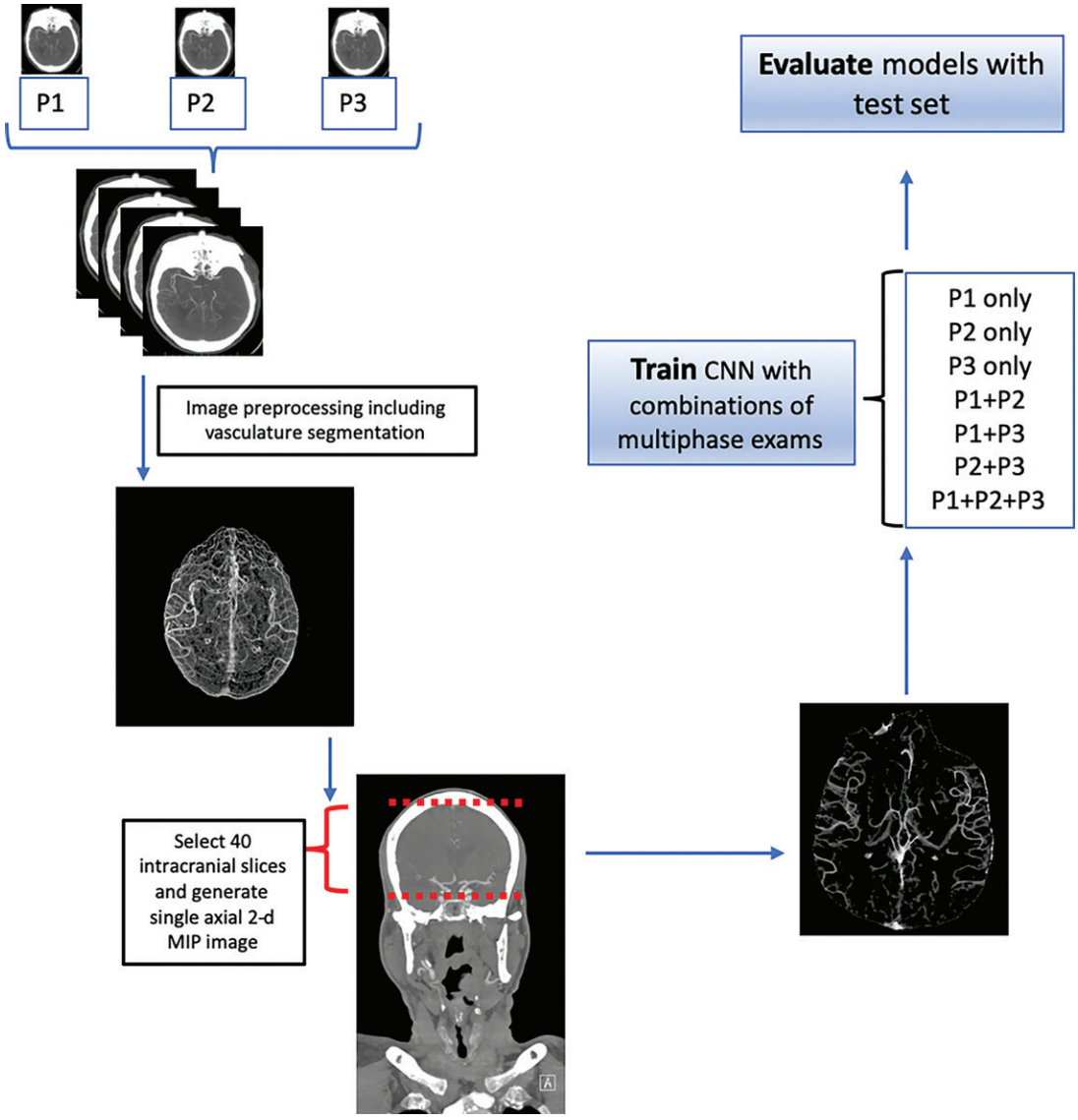

Figure 2: Flowchart demonstrates data preprocessing and experimental setup. The three phases (P1, P2, and P3) of the multiphase examination each underwent a preprocessing pipeline that included vasculature segmentation. Because the relevant information was contained in the downstream intracranial vasculature, we selected the 40 most-cranial axial slices from the circle of Willis to the skull vertex. These 40 axial slices were then converted into a single axial two-dimensional (2-d) maximum intensity projection (MIP) image as the input to our convolutional neural network (CNN). A total of seven experimental combinations were performed and each model was evaluated on the held-out test set.

optimal cutoffs are provided in Table E1 (online) along with Youden values and Hosmer-Lemeshow *P* values.

Given the results of the test set, the use of phases 1 and 3 achieved a significant increase in diagnostic performance relative to using phase 1 alone. The relationship between the prediction of phases 1 and 3 and actual presence of LVO is illustrated in Figure 5. As can be seen in Figure 5, there is a single value that the model predicted to be 100% positive for LVO (lower right-hand corner), although this case had been deemed an actual negative finding. This single false-positive finding was investigated further, revealing no evidence of LVO on the CT angiography image. However, the patient's subsequent MRI, performed 6 hours later, showed a small acute ischemic infarct in the left paramedian pons (Fig 6). A sample case demonstrating multiphase maximum intensity projection CT angiography images is shown in Figure 3.

Discussion

We developed a deep learning model that can classify large vessel occlusions (LVO) on CT angiography images with a high diagnostic performance, achieving an area under the receiver operating characteristic curve (AUC) of 0.89 by using the combination of phases 1, 2, and 3. Our model was discriminative across patient demographics, multiple institutions, and scanners and detected both anterior and posterior circulation occlusions, indicating it could function as a tool to prioritize the review of patients with potential LVO by radiologists and clinicians in the emergency setting. We also established that a model using single-phase CT angiography could achieve an AUC of at least 0.70 whereas models using phases 1 and 3, phases 2 and 3, and phases 1, 2, and 3 could achieve a significant improvement in AUC compared with single phase.

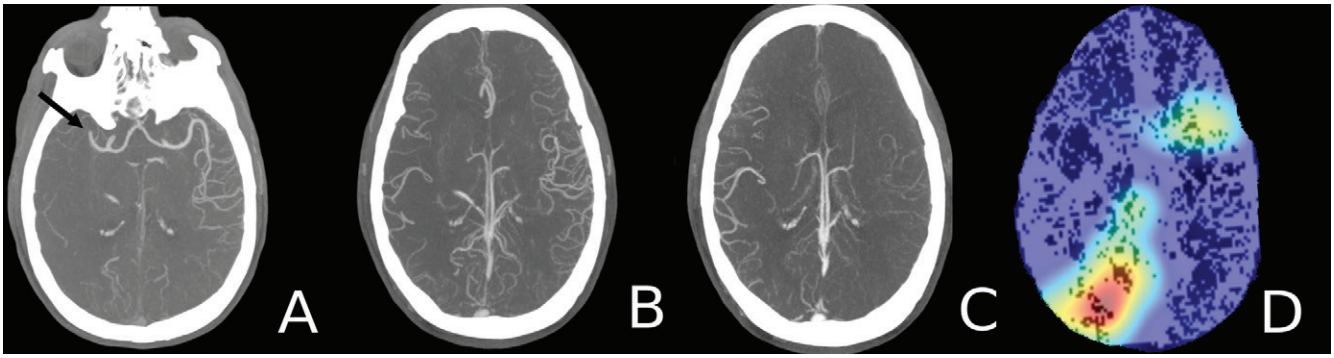

Figure 3: Axial maximum intensity projection images and a heat map in a 60-year old man who presented to the emergency department with new onset left-sided weakness. *A*, Arterial (phase 1) image shows an abrupt occlusion of the distal M1 branch of the right middle cerebral artery (arrow) with paucity of distal vasculature. *B*, Venous (phase 2) image shows subtle asymmetry with minimal increased vascularity in the contralateral left hemisphere. *C*, Late venous (phase 3) image shows prominent increased opacification of the ipsilateral right hemispheric vasculature downstream from the occlusion. *D*, Heat map shows the most discriminative region (red) that the model used for the correct prediction.

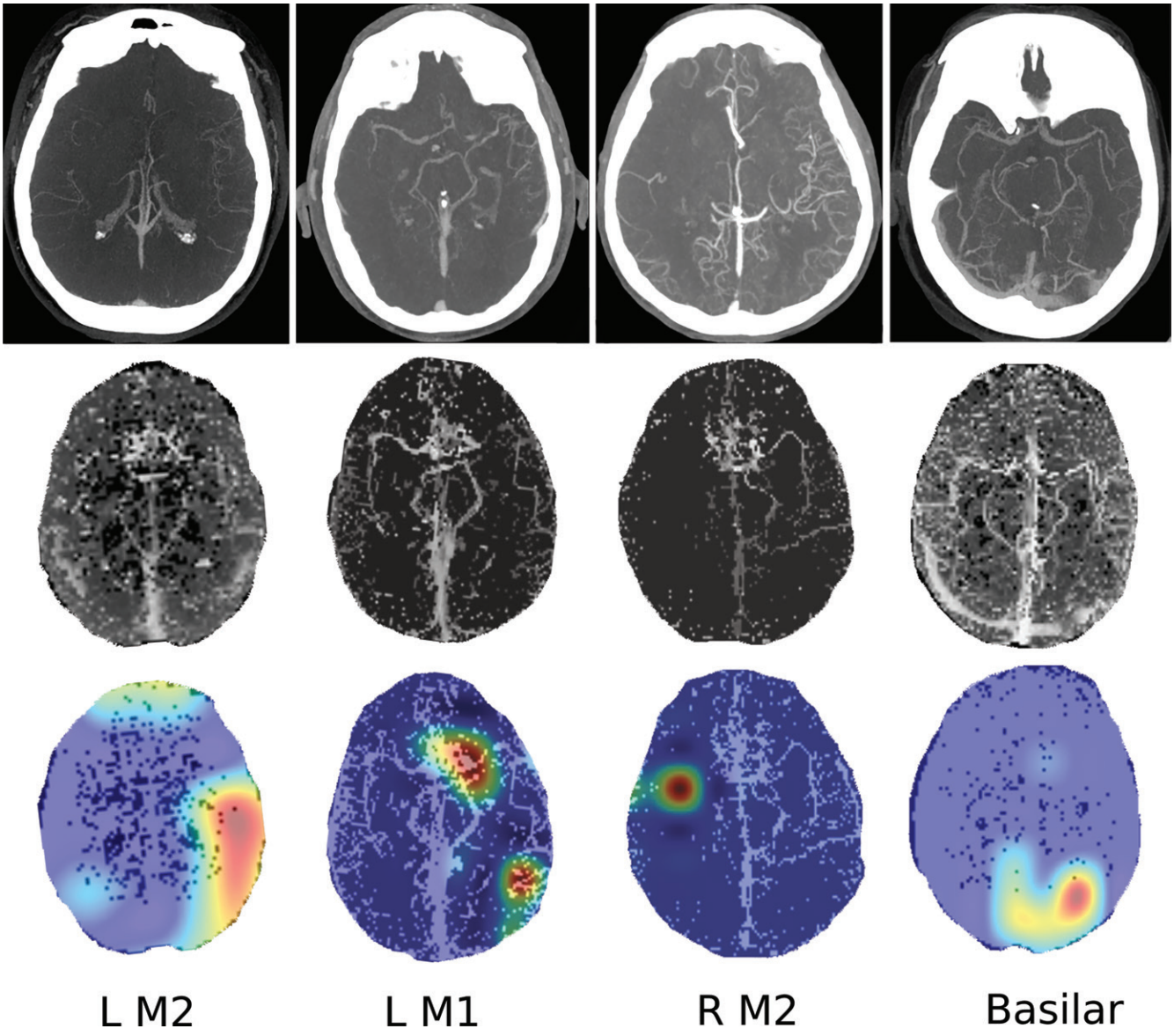

Figure 4: Images show four separate patients with large vessel occlusions correctly predicted by the algorithm. The top row shows a representative CT slice from the delayed venous phase CT angiography. The middle row shows the preprocessed maximum intensity projection images that function as the input to the model. The bottom row are overlaid heat maps, with areas in red showing the most discriminative regions. Notice these so-called hot regions correlate with the occlusion location (respectively: left [L] M2, L M1, right [R] M2, basilar) in each patient.

Table 2: Sensitivity, Specificity, and Area Under the Curve between Validation and Test Sets with Cutoffs by Phase Combination

	Validation Test by Using Cutoffs				Test Set by Using Validation Cutoffs			
Parameter	Sensitivity	Specificity	AUC	*P* Value (reference, phase 1)	Sensitivity	Specificity	AUC	*P* Value (reference, phase 1)
Phase 1	18/27 (67) [47, 82]	23/27 (85) [66, 94]	0.76 [0.65, 0.87]		24/31 (77) [59, 89]	22/31 (71) [53, 84]	0.74 [0.63, 0.85]	
Phase 2	23/27 (85) [66, 94]	24/27 (89) [70, 96]	0.87 [0.78, 0.96]	.051	24/31 (77) [59, 89]	29/31 (94) [77, 98]	0.85 [0.77, 0.94]	.06
Phase 3	25/27 (93) [74, 98]	17/27 (62) [43, 79]	0.78 [0.67, 0.88]	.40	30/31 (96) [80, 100]	16/31 (54) [37, 71]	0.77 [0.67, 0.87]	.33
Phase 1 and 2	25/27 (93) [74, 98]	19/27 (70) [50, 85]	0.81 [0.71, 0.92]	.22	30/31 (97) [80, 100]	21/31 (68) [49, 82]	0.82 [0.73, 0.91]	.12
Phase 1 and 3	25/27 (93) [74, 98]	23/27 (85) [66, 94]	0.89 [0.80, 0.97]	.01	31/31 (100) [0, 100]	22/31 (71) [53, 84]	0.85 [0.77, 0.94]	.03
Phase 2 and 3	23/27 (85) [66, 94]	22/27 (81) [62, 92]	0.81 [0.71, 0.92]	.20	26/31 (84) [66, 93]	27/31 (87) [70, 95]	0.85 [0.77, 0.94]	.03
Phase 1, 2, and 3	26/27 (96) [77, 100]	22/27 (81) [62, 92]	0.89 [0.81, 0.97	.01	31/31 (100) [0, 100]	24/31 (77) [59, 89]	0.89 [0.81, 0.96]	<.01

Note.—Sensitivity and specificity data are numerator/denominator. Data in parentheses are percentages; data in brackets are the 95% confidence interval of the percentage. Phase 1 indicates arterial, phase 2 is peak venous, and phase 3 is late venous. See Table E1 (online) for model fitting and cutoff values. AUC = area under the receiver operating characteristic curve.

Whereas there are several U.S. Food and Drug Administration–approved commercial platforms that use deep learning solutions for automated LVO stroke detection (ie, rapid CT angiography [*https://www.rapidai.com*] and Viz.ai [*https://www.viz.ai*), to our knowledge, this is the first study to use a convolutional neural network to identify LVO by using multiphase CT angiography images. Published results evaluating these commercial platforms that used single-phase CT angiography examinations demonstrated an overall AUC, sensitivity, and specificity of 0.86, 0.92, and 0.81, respectively, for the rapid CT angiography algorithm (28) and sensitivity of 0.82 and specificity of 0.94 for the Viz.ai algorithm (29). However, our study achieved an overall AUC of 0.97 without cutoffs, sensitivity of 1.00, and specificity of 0.77. Additionally, we used multiphase CT angiography images and included posterior circulation and extracranial (cervical) ICA occlusions, whereas the aforementioned studies included only intracranial anterior circulation LVOs and single-phase CT angiography images. Including posterior circulation occlusions is essential to any LVO detector because nearly 20% of ischemic strokes occur in the vertebrobasilar vascular distribution. Furthermore, accurate detection of basilar artery occlusions is paramount given the high morbidity and mortality (30,31).

Because our data set included multiphase CT angiography images, we were able to investigate the role of delayed CT angiography in our model's performance with three separate time-resolved data points. Multiphase CT angiography has been shown to clearly and accurately depict LVO while providing a more nuanced assessment of the intracranial pial collateral network of both the normal hemisphere and the hemisphere with LVO (12,32), with collateral vessels becoming progressively apparent from early to delayed phases (33). This suggests that the best-performing models relied more on asymmetric vascular opacification of vessels distal to an occlusion (ie, the delayed vessel sign [34]), rather than the absence or diminished opacification at the initial arterial phase. Our study found when additional delayed phases were combined with phase 1 (ie, phases 1 and 3 and phases 1, 2, and 3), there was an additive effect resulting in better model performance over single-phase CT angiography indicating that both initial absence of opacification and delayed enhancement are important. Additionally, the phenomenon of downstream asymmetrically

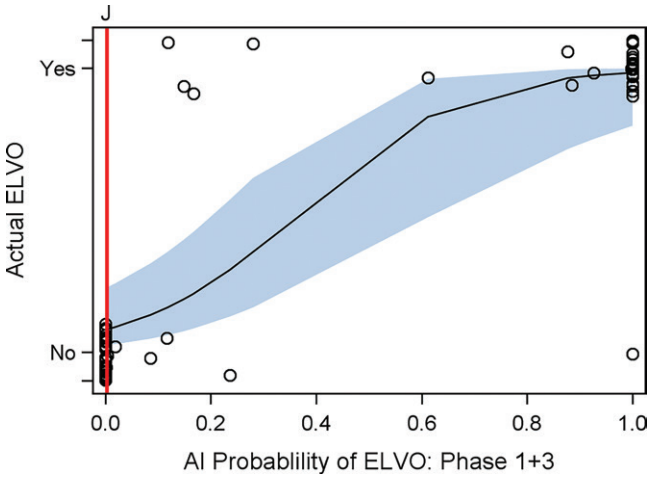

Figure 5: Graph shows artificial intelligence (AI) large vessel occlusion (LVO) prediction score versus presence or absence of LVO for the combination of phase 1 and 3 (arterial and late venous phase). Y-axis represents the binary ground truth of presence or absence of LVO. The x-axis shows the probability range (from 0 to 1.0) of the model predicting the presence of LVO. The solid black line represents the relationship between the likelihood of presence or absence of LVO and prediction score (slope), while the light blue band represents the 95% confidence band of the slope. The red line corresponds to the Youden *J* cutoff value. The circles represent observed data points. ELVO = emergent LVO.

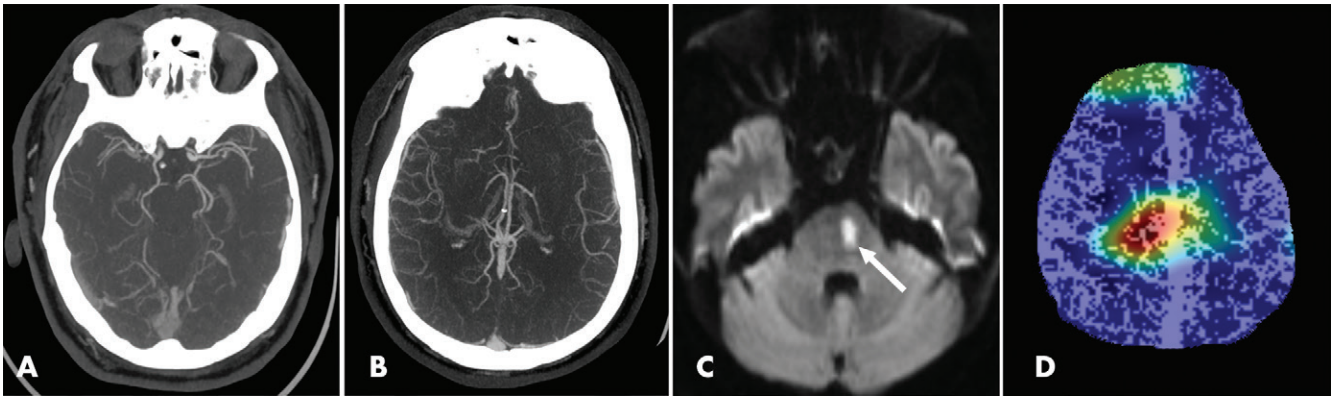

Figure 6: Images show false-positive finding prediction in a 52-year-old man who presented with acute stroke symptoms to the emergency department. *A*, Axial arterial phase CT angiography and, *B*, axial venous phase CT angiography images show no evidence of a large vessel occlusion. Additional noncontrast-enhanced brain CT images (not shown) did not show evidence of acute infarct. *C*, Diffusion-weighted MRI performed 6 hours after presentation shows an area of restricted diffusion consistent with an acute infarct in the left paramedian pons (arrow). *D*, Heat map overlay shows focal activity projecting over the central brain.

increased opacification may explain why our model was able to detect the presence of occlusions located out of the field of view (ie, cervical ICA and vertebrobasilar occlusions) because the z-axis provided to the model spanned only from the circle of Willis to the skull vertex. However, the observed improvements in model performance when using additional phases where limited to comparisons with phase 1 alone only; therefore, these improvements can only be interpreted relative to single-phase CT angiography. Nonetheless, the statistically significant improvements all demonstrated an increase in AUC higher than 0.05 (between 0.11 and 0.15), a commonly accepted goal. Without further investigation, it should not be assumed that an individual phase (ie, the lowest performing phase 2) is detrimental to model performance.

Interestingly, the one incorrectly predicted outlier in our test set was a true-negative LVO, with our classifier predicting it to be positive for LVO with a near 100% probability score. Whereas there was no evidence of LVO at CT angiography, the patient's subsequent MRI approximately 6 hours later showed a small acute ischemic infarct in the left paramedian pons (Fig 6), raising the possibility that our model does not discriminate between the arbitrary categorization of large and small vessel occlusions and may be able to detect smaller vasculature infarcts that human radiologists might not be able to view at CT angiography. This ability of computer vision pipelines to extract new knowledge from medical image data not previously thought to be quantifiable has been documented in other studies, for example, predicting patient sex and age from retinal images (35). Further study would be needed to develop this potential application.

The ultimate test of any machine learning application in radiology is its ability to provide clinical value. Whereas our machine algorithm demonstrates a high performance in detecting LVO, so do radiologists. It had been shown that the diagnostic performance in detecting LVO at CT angiography is high across all levels of radiologist expertise (sensitivity and specificity both >0.94), with expertise ranging from radiology residents to fellowship-trained neuroradiologists (36). However, an algorithm that can detect LVO with high fidelity could augment its human counterpart by offering a so-called consult for difficult cases. Additionally, cases with positive findings could immediately get flagged, leading to faster mobilization of teams for endovascular therapy.

The strengths of our study include a varied patient population from multiple hospitals and CT scanners with variations in technical parameters (37). Also, additional head and neck vasculature pathology was not excluded in either the LVO-positive or LVO-negative cohorts. This heterogeneity suggests the results could be applied generally in the clinical setting. Additionally, our ground truth for the presence of LVO comes from subsequent diagnostic cerebral angiographic confirmation performed by fellowship-trained neurointerventional radiologists. Finally, our model incorporates both anterior and posterior circulation occlusions, making this a robust tool for detecting all subtypes of potential LVOs eligible for mechanical thrombectomy.

Our study had several limitations. Our cohort of positive cases was relatively small for deep learning, which limits the subset analysis of a particular class of occlusion (ie, M1, M2, and ICA). Thus, we were only able to analyze whether an LVO was present or not within a given patient. Further studies with more examples of each occlusion location are needed to obtain a more granular picture of how well the model performs for given occlusion locations. Second, we optimized our model with as many examples of LVO-positive findings as possible while matching with an equal number of examples of LVO-negative findings regarding age and sex. This was done to maximize sensitivity and specificity because our data set consisted of an artificially high LVO prevalence. Therefore, we were unable to estimate accurate positive or negative predictive values. However, because real-world LVO prevalence is much lower than 50%, our already high negative predictive value (due to high sensitivity) would remain at or near 100% in real-world settings, which is arguably the more important feature. Additionally, this was a retrospective study with data obtained from three local hospitals. A prospective evaluation of our model with an external geographically more diverse patient population would ensure reproducibility and increase generalizability. Third, our model only provided a probability score for the

global presence or absence of an LVO and does not segment or identify the location of LVO, which would be helpful for a radiologist who uses this in a clinical setting. In addition, our model was only able to perform the single task of detecting LVO on CT angiography images. Additional classifiers would have to be added to detect alternative acute intracranial pathology (such as intracranial hemorrhage or aneurysm) if this technology were to be used as a comprehensive triage tool in the emergency setting because acute ischemic stroke–like symptoms can be a manifestation of alternative pathology. Evaluation of diagnostic performance was limited to sensitivity and specificity because our prevalence was artificial (ie, we powered for sensitivity and specificity equally given the small true population prevalence of positives); thus, we could not evaluate positive and negative predictive value. A prospective evaluation of our model in the emergency setting is the next step to evaluate its clinical utility. Finally, there was no overt evidence of model overfitting, a common problem in machine learning, because the performance of the test set matched closely with the validation set. The observation of a drop in AUC within the validation with phase 2 (compared with combinations of phase 1 and 2 and phase 2 and 3) likely reflected a performance variation with additional added data (ie, phases) providing the very high dimensional input feature space of our model.

In conclusion, we successfully developed a deep learning convolutional neural network to detect large vessel occlusion at multiphase CT angiography with a high area under the receiver operating characteristic curve, particularly when using delayed phases. Our work is an important first step in incorporating deep learning to triage large vessel occlusions (LVOs) in the emergency setting and has the potential to shorten the time to LVO detection with ultimate improvements in patient outcomes.

Acknowledgment: The authors acknowledge Luke Zhu for his technologic expertise and organizational assistance.

Author contributions: Guarantors of integrity of entire study, M.T.S., S.S.S., A.W., R.A.M.; study concepts/study design or data acquisition or data analysis/interpretation, all authors; manuscript drafting or manuscript revision for important intellectual content, all authors; approval of final version of submitted manuscript, all authors; agrees to ensure any questions related to the work are appropriately resolved, all authors; literature research, M.T.S., J.V., M.P.D., S.S.S., A.W., H.L.C.W., A.D.Y., C.E., R.A.M.; clinical studies, M.T.S., A.D.Y., J.L.B., R.A.M.; experimental studies, M.T.S., J.V., Y.H.K., S.S.S., H.J.T., A.W., H.L.C.W., C.E., U.C.; statistical analysis, M.T.S., J.V., M.P.D., S.S.S., H.J.T., A.W., H.L.C.W., M.J., G.L.B.; and manuscript editing, M.T.S., J.V., M.P.D., S.S.S., H.J.T., A.W., H.L.C.W., A.D.Y., M.J., J.L.B., C.E., J.L.B., R.A.M.

Disclosures of Conflicts of Interest: **M.T.S.** disclosed no relevant relationships. **J.V.** disclosed no relevant relationships. **M.P.D.** disclosed no relevant relationships. **Y.H.K.** disclosed no relevant relationships. **S.S.S.** disclosed no relevant relationships. **H.J.T.** Activities related to the present article: disclosed summer stipend to work on this subject from UTRA. Activities not related to the present article: disclosed no relevant relationships. Other relationships: disclosed no relevant relationships. **A.W.** disclosed no relevant relationships. **H.L.C.W.** disclosed no relevant relationships. **A.D.Y.** disclosed no relevant relationships. **M.J.** Activities related to the present article: disclosed no relevant relationships. Activities not related to the present article: disclosed one-time speaking fee from Medtronic. Other relationships: disclosed no relevant relationships. **J.L.B.** disclosed no relevant relationships. **C.E.** Activities related to the present article: disclosed no relevant relationships. Activities not related to the present article: disclosed grants from DARPA and IARPA. Other relationships: disclosed no relevant relationships. **U.C.** disclosed no relevant relationships. **G.L.B.** disclosed no relevant relationships. **R.A.M.** disclosed no relevant relationships.

References

1. Albers GW, Marks MP, Kemp S, et al. Thrombectomy for Stroke at 6 to 16 Hours with Selection by Perfusion Imaging. N Engl J Med 2018;378(8):708–718.
2. Berkhemer OA, Fransen PSS, Beumer D, et al. A Randomized Trial of Intraarterial Treatment for Acute Ischemic Stroke. N Engl J Med 2015;372(1):11–20 [Published correction appears in N Engl J Med 2015;372(4):394.].
3. Campbell BCV, Mitchell PJ, Kleinig TJ, et al. Endovascular Therapy for Ischemic Stroke with Perfusion-Imaging Selection. N Engl J Med 2015;372(11):1009–1018.
4. Goyal M, Demchuk AM, Menon BK, et al. Randomized Assessment of Rapid Endovascular Treatment of Ischemic Stroke. N Engl J Med 2015;372(11):1019–1030.
5. Jovin TG, Chamorro A, Cobo E, et al. Thrombectomy within 8 Hours after Symptom Onset in Ischemic Stroke. N Engl J Med 2015;372(24):2296–2306.
6. Nogueira RG, Jadhav AP, Haussen DC, et al. Thrombectomy 6 to 24 Hours after Stroke with a Mismatch between Deficit and Infarct. N Engl J Med 2018;378(1):11–21.
7. Saver JL, Goyal M, Bonafe A, et al. Stent-Retriever Thrombectomy after Intravenous t-PA vs. t-PA Alone in Stroke. N Engl J Med 2015;372(24):2285–2295.
8. Meretoja A, Keshtkaran M, Tatlisumak T, Donnan GA, Churilov L. Endovascular therapy for ischemic stroke: Save a minute-save a week. Neurology 2017;88(22):2123–2127.
9. Deipolyi AR, Hamberg LM, Gonzaléz RG, Hirsch JA, Hunter GJ. Diagnostic yield of emergency department arch-to-vertex CT angiography in patients with suspected acute stroke. AJNR Am J Neuroradiol 2015;36(2):265–268.
10. Mayer SA, Viarasilpa T, Panyavachiraporn N, et al. CTA-for-All: Impact of Emergency Computed Tomographic Angiography for All Patients With Stroke Presenting Within 24 Hours of Onset. Stroke 2020;51(1):331–334.
11. McTaggart RA, Ansari SA, Goyal M, et al. Initial hospital management of patients with emergent large vessel occlusion (ELVO): report of the standards and guidelines committee of the Society of NeuroInterventional Surgery. J Neurointerv Surg 2017;9(3):316–323.
12. Menon BK, d'Esterre CD, Qazi EM, et al. Multiphase CT Angiography: A New Tool for the Imaging Triage of Patients with Acute Ischemic Stroke. Radiology 2015;275(2):510–520.
13. Yu AYX, Zerna C, Assis Z, et al. Multiphase CT angiography increases detection of anterior circulation intracranial occlusion. Neurology 2016;87(6):609–616.
14. Almekhlafi MA, Kunz WG, McTaggart RA, et al. Imaging Triage of Patients with Late-Window (6-24 Hours) Acute Ischemic Stroke: A Comparative Study Using Multiphase CT Angiography versus CT Perfusion. AJNR Am J Neuroradiol 2020;41(1):129–133.
15. Russakovsky O, Deng J, Su H, et al. Imagenet large scale visual recognition challenge. Int J Comput Vis 2015;115(3):211–252.
16. Qi Dou, Hao Chen, Lequan Yu, et al. Automatic Detection of Cerebral Microbleeds From MR Images via 3D Convolutional Neural Networks. IEEE Trans Med Imaging 2016;35(5):1182–1195.
17. Chen L, Bentley P, Rueckert D. Fully automatic acute ischemic lesion segmentation in DWI using convolutional neural networks. Neuroimage Clin 2017;15:633–643.
18. Qiu W, Kuang H, Teleg E, et al. Machine Learning for Detecting Early Infarction in Acute Stroke with Non-Contrast-enhanced CT. Radiology 2020;294(3):638–644.
19. Arbabshirani MR, Fornwalt BK, Mongelluzzo GJ, et al. Advanced machine learning in action: identification of intracranial hemorrhage on computed tomography scans of the head with clinical workflow integration. NPJ Digit Med 2018;1(1):9https://doi.org/10.1038/s41746-017-0015-z.
20. Buda M, Maki A, Mazurowski MA. A systematic study of the class imbalance problem in convolutional neural networks. Neural Netw 2018;106:249–259.
21. Braovic M, Stipanicev D, Seric L. Retinal blood vessel segmentation based on heuristic image analysis. Comput Sci Inf Syst 2019;16(1):227–245.
22. Chollet F. Xception: Deep Learning with Depthwise Separable Convolutions. 2017 IEEE Conference on Computer Vision and Pattern Recognition (CVPR). In: 2017 IEEE Conference on Computer Vision and Pattern Recognition (CVPR), Honolulu, HI, July 21–26, 2017. Piscataway, NJ: IEEE, 2017; 1800–1807.
23. Szegedy C, Vanhoucke V, Ioffe S, Shlens J, Wojna Z. Rethinking the Inception Architecture for Computer Vision. arXiv:1512.00567 [cs]. http://arxiv.org/abs/1512.00567. Posted 2015. Accessed May 25, 2019.
24. He K, Zhang X, Ren S, Sun J. Deep Residual Learning for Image Recognition. arXiv:1512.03385 [cs]. http://arxiv.org/abs/1512.03385. Posted 2015. Accessed January 19, 2020.
25. Simonyan K, Zisserman A. Very Deep Convolutional Networks for Large-Scale Image Recognition. arXiv:1409.1556 [cs]. https://arxiv.org/abs/1409.1556. Posted 2015.
26. Huang G, Liu Z, van der Maaten L, Weinberger KQ. Densely Connected Convolutional Networks. arXiv:1608.06993 [cs]. http://arxiv.org/abs/1608.06993. Posted 2016. Accessed May 25, 2019.
27. Selvaraju RR, Cogswell M, Das A, Vedantam R, Parikh D, Batra D. Grad-CAM: Visual Explanations from Deep Networks via Gradient-based Localization. Int J Comput Vis 2020;128(2):336–359.
28. Amukotuwa SA, Straka M, Smith H, et al. Automated Detection of Intracranial Large Vessel Occlusions on Computed Tomography Angiography: A Single Center Experience. Stroke 2019;50(10):2790–2798.
29. Chatterjee A, Somayaji NR, Kabakis IM. Abstract WMP16: Artificial Intelligence Detection of Cerebrovascular Large Vessel Occlusion - Nine Month, 650 Patient Evaluation of the Diagnostic Accuracy and Performance of the Viz.ai LVO Algorithm. Stroke 2019;50(Suppl_1):WMP16.
30. Lindsberg PJ, Mattle HP. Therapy of basilar artery occlusion: a systematic analysis comparing intra-arterial and intravenous thrombolysis. Stroke 2006;37(3):922–928.
31. Smith E, Delargy M. Locked-in syndrome. BMJ 2005;330(7488):406–409.

32. Lima FO, Furie KL, Silva GS, et al. Prognosis of untreated strokes due to anterior circulation proximal intracranial arterial occlusions detected by use of computed tomography angiography. JAMA Neurol 2014;71(2):151–157.
33. Frölich AMJ, Wolff SL, Psychogios MN, et al. Time-resolved assessment of collateral flow using 4D CT angiography in large-vessel occlusion stroke. Eur Radiol 2014;24(2):390–396.
34. Byrne D, Sugrue G, Stanley E, et al. Improved Detection of Anterior Circulation Occlusions: The "Delayed Vessel Sign" on Multiphase CT Angiography. AJNR Am J Neuroradiol 2017;38(10):1911–1916.
35. Poplin R, Varadarajan AV, Blumer K, et al. Prediction of cardiovascular risk factors from retinal fundus photographs via deep learning. Nat Biomed Eng 2018;2(3):158–164.
36. Boyd CA, Jayaraman MV, Baird GL, et al. Detection of emergent large vessel occlusion stroke with CT angiography is high across all levels of radiology training and grayscale viewing methods. Eur Radiol 2020;30(8):4447–4453.
37. Park SH, Han K. Methodologic Guide for Evaluating Clinical Performance and Effect of Artificial Intelligence Technology for Medical Diagnosis and Prediction. Radiology 2018;286(3):800–809.